Orientation as a probe of photodissociation dynamics

Zee Hwan Kim, Andrew J. Alexander, S. Alex Kandel,† T. Peter Rakitzis‡ and Richard N. Zare*

Department of Chemistry, Stanford University, Stanford, CA 94305, USA

Received 9th March 1999

Molecular chlorine (Cl_2) was photodissociated in the wavelength range 270–400 nm with linearly polarized light, and the orientation of the excited-state chlorine atom $Cl^*(^2P_{1/2})$ was measured by 2 + 1 resonance enhanced multiphoton ionization (REMPI) using circularly polarized light. The degree of orientation of the Cl* photofragment is found to oscillate as a function of photolysis wavelength. The oscillation is a result of quantum mechanical coherence arising from electronic states of different symmetry that correlate to the same separated-atom asymptote. A simple curve-crossing model using *ab initio* potential energy curves reproduces the general shape of the oscillation but fails to give a quantitative fit.

1. Introduction

Atomic and molecular photofragment vector properties have fascinated physical chemists since the early days of gas-phase reaction dynamics. The vector properties associated with molecular photodissociation provide insight not usually available from their scalar counterparts. For example, the correlation of the fragment recoil velocity with the polarization of the photolysis light provides information about the symmetry of the initially excited dissociating state.[1] This correlation is usually expressed by the translational anisotropy parameter β, which ranges from $+2$ for a pure parallel transition to -1 for a pure perpendicular transition. Intermediate values of β indicate a transition of mixed parallel and perpendicular character within the axial recoil approximation. Unfortunately, measurement of the photofragment translational anisotropy is not a sensitive diagnostic of the dynamics that occur after the initial excitation. Instead, as we show, measurement of the correlation of the angular momentum vector of an atomic or molecular photofragment with respect to its recoil velocity vector can provide important information for understanding the dynamics of photodissociation far from the Franck–Condon region.

There have been extensive theoretical and experimental studies of photofragment angular momentum polarization.[2,3] Dixon formulated a semiclassical description of photofragment angular momentum polarization using bipolar moments measured in the laboratory frame, and showed how to extract these parameters from the analysis of Doppler-broadened line shapes.[2] The quantum mechanical nature of angular momentum polarization manifests itself in effects such as coherence and interference between the photofragment quantum states: these effects are more

† Present address: Department of Chemistry, The Pennsylvania State University, 152 Davey Laboratory, University Park, PA 16802, USA.

‡ Present address: Department of Chemistry, University of Crete and Institute of Electronic Structure and Laser, Foundation for Research and Technology-Hellas, 71110 Heraklion-Crete, Greece.

pronounced in the case of atomic photofragments owing to the low angular momentum quantum numbers. In 1968, van Brunt and Zare[4] predicted that atomic photofragments could be polarized. Full quantum mechanical treatments of photofragment polarization, allowing for mixed transitions and photofragment coherence, have been given by Vasyutinskii,[5] Siebbeles *et al.*,[6] and by Chen and Pei.[7] Several experiments have since demonstrated the polarization of atomic fragments and quantum mechanical effects.[8-11] For example, Vigué *et al.*[10] observed the anomalous polarized emission from Ca atoms in Ca_2 photodissociation, which can be explained by a coherent excitation of $\Lambda = 1$ and $\Lambda = -1$ states. More recently, Eppink *et al.*[11] reported the production of maximally aligned O (^{1}D) atoms in the photodissociation of O_2.

Rakitzis and Zare[12] showed how to measure the complete photofragment angular momentum distribution in the molecular frame using the specialized polarization parameters $\boldsymbol{a}_q^{(k)}(\parallel)$, $\boldsymbol{a}_q^{(k)}(\perp)$, and $\boldsymbol{a}_q^{(k)}(\parallel,\perp)$. The $\boldsymbol{a}_q^{(k)}$ parameters are decoupled from the translational anisotropy of the fragments, to provide a clear physical picture of the dissociation process. Furthermore, the $\boldsymbol{a}_q^{(k)}$ formalism explicitly accounts for contributions from the coherence between photofragments associated with repulsive states of different symmetry [$\boldsymbol{a}_q^{(k)}(\parallel,\perp)$], as well as individual contributions from parallel [$\boldsymbol{a}_q^{(k)}(\parallel)$] and perpendicular [$\boldsymbol{a}_q^{(k)}(\perp)$] transitions. The power of using the $\boldsymbol{a}_q^{(k)}$ formalism was demonstrated in measurements of the mass-dependent polarization of the Cl-atom in the photolysis of ICl.[13–15] The large differences in the observed alignment and orientation of (ground-state) ^{35}Cl and ^{37}Cl atoms arise solely from the quantum mechanical interference between two or more dissociating states with different symmetries. In addition, it was demonstrated that it is possible to prepare an atomic photofragment with well-defined helicity (orientation) with respect to the photofragment velocity vector. The measurement of the orientation parameter, $\mathrm{Im}[\boldsymbol{a}_1^{(1)}(\parallel,\perp)]$, as a function of excitation energy was shown to be highly sensitive to the shapes of potential energy curves involved. Consequently, measurement of $\mathrm{Im}[\boldsymbol{a}_1^{(1)}(\parallel,\perp)]$, opens the possibility for this parameter to serve as a powerful probe of molecular photodissociation dynamics. Rakitzis *et al.*[14] discussed the analogy with the famous Young's double slit experiment, in which there is a definite phase relationship between rays of light that have travelled different paths. The phase relationship can provide information on the nature of the paths travelled, and indeed, on the radiation source itself.

For many photodissociation processes, nonadiabatic interactions—resulting from a breakdown of the Born–Oppenheimer approximation—may have a significant influence on the photofragmentation dynamics. Unfortunately, it is not straightforward to obtain detailed information on the nature of nonadiabatic interactions from more traditional experiments, such as measurements of fine structure branching ratios or angular distributions of the products. The measurement of the orientation parameter, however, can reveal important information on the nature of nonadiabatic interactions. The nonadiabatic interactions influence the phases as well as the amplitudes of the dissociating wave functions and so the $\mathrm{Im}[\boldsymbol{a}_1^{(1)}(\parallel,\perp)]$, which is sensitive to the asymptotic phase difference between these dissociating wave functions, can carry a "fingerprint" of the nonadiabatic interaction.

Nonadiabatic interactions have been shown to occur in the molecular photodissociation of Cl_2 around 330 nm.[16,17] The major channel for the photodissociation of Cl_2 at this wavelength is *via* the $C\,^1\Pi_u(1) - X\,^1\Sigma_g^+(0^+)$ ($|\Delta\Omega| = 1$) perpendicular transition, which adiabatically correlates to ground-state Cl ($^2P_{3/2}$) + Cl ($^2P_{3/2}$) atoms. At longer excitation wavelengths, around 430 nm, absorption is dominated by the $B\,^3\Pi_u^+(0^+) - X\,^1\Sigma_g^+(0^+)$ ($|\Delta\Omega| = 0$) parallel transition, which adiabatically correlates to Cl*($^2P_{1/2}$) + Cl ($^2P_{3/2}$): see Fig. 1. Matsumi *et al.*[16] used Doppler spectroscopy to measure the translational anisotropy of chlorine atomic fragments, and noted a gradual change of the β parameter of Cl* as a function of excitation wavelength. At a photolysis wavelength of 400 nm, β(Cl*) was measured to be close to 2, which allowed them to assign the photodissociation process to the $B\,^3\Pi_u^+(0^+) - X\,^1\Sigma_g^+(0^+)$ parallel transition, whereas at 308 nm, β(Cl*) was found to be -0.7, which indicated the existence of a perpendicular transition resulting in production of Cl*. They attributed the perpendicular transition component as initial excitation to the C state followed by radial derivative coupling to other states of the same symmetry, with two of the states correlating to the Cl + Cl* channel. Recently, Samartzis *et al.*[17] have refined previous measurements of the Cl* translational anisotropy using the velocity-mapped photofragment imaging technique. They attributed the perpendicular portion of the Cl* fragments to initial excitation of the C state followed by curve crossing to the B state, which correlates with Cl + Cl*.

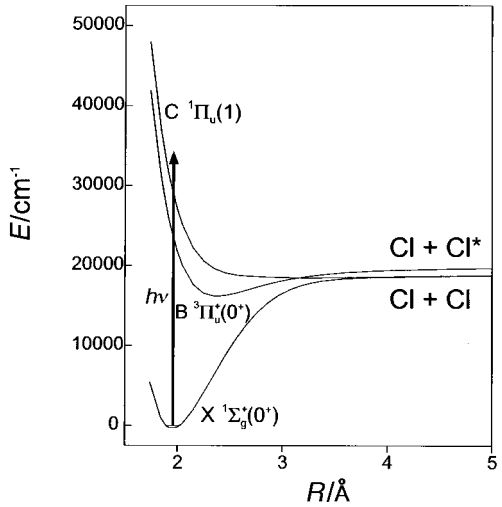

Fig. 1 *Ab initio* potential energy curves[18] of Cl_2 relevant to the present discussion. Excitation to the C state is a perpendicular transition and correlates adiabatically to ground-state Cl + Cl. Excitation to the B state is a parallel transition and correlates adiabatically to Cl + Cl*. The *ab initio* B and C state potential energy curves cross each other at 3.16 Å.

The curve crossing probability, which they estimated using a combined analysis of measurements of the ground-state Cl fragment velocity distribution and measurements of β(Cl*), was found to decrease with an increase in available energy. This finding supports their assumption of a curve crossing mechanism, of the Landau–Zener type, from the C to the B state. In summary, two recent experimental works have indicated the importance of nonadiabatic interactions in the photodissociation of Cl_2 around 330 nm. However, the mechanism for the nonadiabatic transition has yet to be fully characterized.

In this discussion, we report measurements of the orientation moment $\mathrm{Im}[\boldsymbol{a}_1^{(1)}(\parallel,\perp)]$ of the excited-state chlorine atom ($^2P_{1/2}$, Cl*) in the photodissociation of Cl_2 using linearly polarized photolysis light (270–400 nm), and circularly polarized probe light for detection of the product atoms. In the intermediate region of excitation wavelengths employed (around 330 nm) the parallel and perpendicular transition components leading to Cl + Cl* products contribute in comparable amounts. The orientation of Cl* photofragments arises from quantum mechanical interference between products originating from the mixed parallel/perpendicular transition.

2. Detection of photofragment angular momentum polarization

Using the formalism of Rakitzis and Zare,[12] the polarization of an ensemble of Cl* ($J = 1/2$) fragments can be fully described by only two moments, with $k = 0$ (isotropic moment, proportional to the population) and $k = 1$ (orientation moment). Orientation of photofragments *via* photolysis with linearly polarized light can arise only from quantum interference between parallel and perpendicular transitions. In addition, the use of linearly polarized photolysis light allows only the existence of the imaginary part of the photofragment orientation parameter, $\mathrm{Im}[\boldsymbol{a}_1^{(1)}(\parallel,\perp)]$. The angular momentum distribution of photofragments with $J = 1/2$ from photodissociation with linearly polarized light is given by

$$D_{\parallel,\perp}(\theta, \varphi, \theta_\varepsilon, \beta) = 1 + \sqrt{2}\,\mathrm{Im}[\boldsymbol{a}_1^{(1)}(\parallel,\perp)]\sin\theta_\varepsilon \cos\theta_\varepsilon \sin\theta \sin\varphi/[1 + \beta P_2(\cos\theta_\varepsilon)] \quad (1)$$

In the molecular frame, the z-axis is defined to lie along the photofragment velocity vector, $\boldsymbol{v}$; see Fig. 2. The polar angle of the photolysis polarization ($\boldsymbol{\varepsilon}_{\mathrm{phot}}$) with respect to the z-axis is given by θ_ε. The xz plane contains both the velocity and the photolysis polarization vectors. θ and φ represent the polar and azimuthal angles of the product angular momentum vector ($\boldsymbol{J}$) with

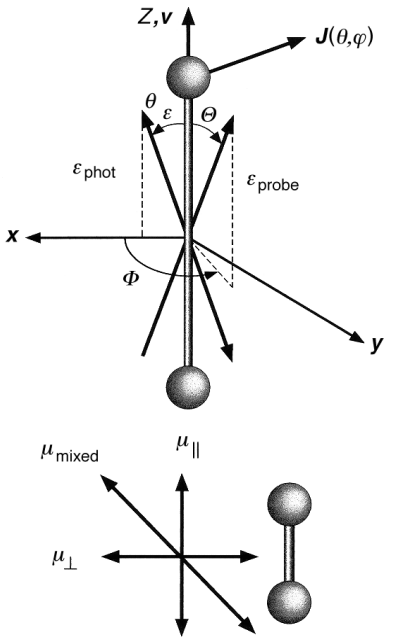

Fig. 2 The molecular frame and coordinates used in this paper. The z-axis is defined by the product photofragment velocity $\boldsymbol{v}$, and the y-axis is normal to the plane containing $\boldsymbol{v}$ and the photolysis polarization vector, $\boldsymbol{\varepsilon}_{\text{phot}}$. θ_ε is the angle between $\boldsymbol{v}$ and $\boldsymbol{\varepsilon}_{\text{phot}}$, Θ and Φ are polar angles of $\boldsymbol{\varepsilon}_{\text{probe}}$ vector, and θ and φ are the polar and azimuthal angles of the photofragment angular momentum ($\boldsymbol{J}$) in the molecular frame.

respect to the molecular frame P_2 is the second-order Legendre polynomial. As can be seen, asymmetry of the distribution with respect to the xz molecular plane occurs for a non-zero $\text{Im}[\boldsymbol{a}_1^{(1)}(\|,\perp)$ moment.

It can be shown that the $\text{Im}[\boldsymbol{a}_1^{(1)}(\|,\perp)]$ moment is proportional to the sine of the asymptotic phase difference ($\Delta\phi = \phi_\perp - \phi_\|$) between the radial parts of the outgoing wavefunctions from parallel and perpendicular transitions, modulated by the product of transition amplitudes for these transitions[5,6,12]:

$$\text{Im}[\boldsymbol{a}_1^{(1)}(\|,\perp)] \propto |A_\||\,|A_\perp|\sin\Delta\phi, \tag{2}$$

where $|A_\||$ and $|A_\perp|$ are the moduli of transition amplitudes for parallel and perpendicular transitions leading to the same product quantum state. For a pure (parallel or perpendicular) transition, the product of the two amplitudes $|A_\||\,|A_\perp|$ in eqn. (2) will be zero, and the $\text{Im}[\boldsymbol{a}_1^{(1)}(\|,\perp)]$ will vanish. The asymptotic phase difference, $\Delta\phi$, and hence the $\text{Im}[\boldsymbol{a}_1^{(1)}(\|,\perp)]$, is sensitive to the kinetic energy available to the photofragments, the shapes of the potential energy pathways encountered for fragments of parallel or perpendicular origin, and therefore, the occurrence (if any) of nonadiabatic interactions for these fragments during the dissociation process.

The REMPI detection of photofragments with polarized light is sensitive to the photofragment angular momentum polarization, and provides a convenient tool for detection of the Cl* atom photofragments. The relative detection probability of Cl* ($J = 1/2$) photofragments using $2 + 1$ REMPI with circularly polarized probe light can be expressed in terms of the $\text{Im}[\boldsymbol{a}_1^{(1)}(\|,\perp)]$ moment:

$$I[\Theta, \Phi, \theta_\varepsilon, \text{Im}[\boldsymbol{a}_1^{(1)}(\|,\perp)] = 1 + \sqrt{2}\,G^1 s_1\,\text{Im}[\boldsymbol{a}_1^{(1)}(\|,\perp)]\sin\theta_\varepsilon\cos\theta_\varepsilon \times \sin\Theta\sin\Phi/[1 + \beta P_2(\cos\theta_\varepsilon)], \tag{3}$$

where G^1 is the long-time limit of nuclear hyperfine depolarization ratio.[19,20] For the excited-state chlorine atom ($J = 1/2$, nuclear spin $I = 3/2$), G^1 is calculated to be 0.375; s_1 is the detection sensitivity[21] for the $k = 1$ moment, which depends on the details of transition of the resonant absorption step, and is calculated to be $-\sqrt{3}$ for the particular transition ($^2\text{P}_{3/2} - {}^2\text{P}_{1/2}$) used.

The angles Θ and Φ specify the direction of the probe radiation polarization vector; see Fig. 2. For the circularly polarized probe light, $\boldsymbol{\varepsilon}_{\mathbf{probe}}$ refers to the direction either parallel (left-circular polarization) or antiparallel (right-circular polarization) to the propagation direction of the light.

3. Experiment

Detailed descriptions of the experimental apparatus and techniques have been given elsewhere,[22] and only a brief overview is given here. Molecular chlorine (Matheson, 99.999%) was premixed with high-purity helium (Liquid Carbonic, 99.995%) in a dilute mixture (less than 5% by volume) before supersonic expansion through a pulsed nozzle (General Valve 9-Series, 0.6 mm orifice) into high vacuum. The stagnation pressure of the sample used was varied from 100 to 400 Torr. The 270–400 nm photolysis light was generated by frequency-doubling the output of a dye laser pumped by a Nd^{3+}: YAG laser (Continuum, ND6000 and PL9020). The probe light (236.53 nm) for 2 + 1 REMPI detection of Cl* *via* the $3s^23p^34p^1\ ^2P_{3/2} - 3s^23p^4\ ^2P_{1/2}$ transition was generated by frequency-doubling the output of a dye laser pumped by a second Nd^{3+}: YAG laser (Spectra-Physics, PDL-3 and DCR-2A; Exciton, Coumarin 480 dye). Photolysis and probe beams were loosely focussed onto the unskimmed expansion within the extraction region of a Wiley-McLaren time-of-flight (TOF) mass spectrometer operated under velocity-sensitive conditions. The relatively high natural abundance of the chlorine-37 isotope (24%) allowed the simultaneous measurement of ^{35}Cl* and ^{37}Cl* ion arrival TOF profiles. The intensities of the photolysis and probe beams were attenuated to avoid unwanted distortion of TOF profiles caused by space charge effects.

Circular polarization of the probe radiation was achieved by placing a quarter-wave plate with its optical axis at 45° with respect to the linear polarization vector of the probe UV light. A photo-elastic modulator (PEM, Hinds International, PEM-80) was placed before the quarter-wave plate to flip the polarization to be either left-circularly polarized (LCP) or right-circularly polarized (RCP) with respect to the propagation axis of the beam on an every-other-shot basis. To achieve maximum sensitivity to the detection of the orientation moment, the polarization of the pump laser was tilted by 45° with respect to the TOF detection axis using a double Fresnel rhomb (Optics for Research, RFU-1/2-U). The time delay between photolysis and probe pulses was kept within 20 ns to avoid unwanted fly-out of photofragments from the detection region. Purity of polarization was found to be critical for these experiments, and therefore care was taken to avoid unwanted distortions of the polarizations of both photolysis and probe beams. TOF profiles taken using left-circularly polarized probe light, $\boldsymbol{I}_{\mathrm{LCP}}$, and right-circularly polarized probe light, $\boldsymbol{I}_{\mathrm{RCP}}$, were recorded separately on a shot-to-shot basis.

Isotropic ($\boldsymbol{I}_{\mathrm{iso}} = \boldsymbol{I}_{\mathrm{LCP}} + \boldsymbol{I}_{\mathrm{RCP}}$), and anisotropic ($\boldsymbol{I}_{\mathrm{aniso}} = \boldsymbol{I}_{\mathrm{LCP}} - \boldsymbol{I}_{\mathrm{RCP}}$) TOF profiles were evaluated and orientation moments extracted by fitting these composite experimental profiles. Isotropic and anisotropic basis functions ($\boldsymbol{B}_{\mathrm{iso}}$ and $\boldsymbol{B}_{\mathrm{aniso}}$) were generated by Monte-Carlo simulation[12] using eqns. (1) and (3). Experimental composite TOF profiles $\boldsymbol{I}_{\mathrm{aniso}}$ and $\boldsymbol{I}_{\mathrm{iso}}$ are least-squares fitted using the following equations:

$$\boldsymbol{I}_{\mathrm{iso}} = c\ \boldsymbol{B}_{\mathrm{iso}}, \tag{4}$$

$$\boldsymbol{I}_{\mathrm{aniso}} = c\ \mathrm{Im}[\boldsymbol{a}_1^{(1)}(\parallel,\perp)]\boldsymbol{B}_{\mathrm{aniso}}, \tag{5}$$

where c is determined by fitting eqn. (4) first. The translational anisotropy parameters β needed for generating the basis functions were taken from the work of Samartzis *et al.*[17] The same β parameter was used for each of the two isotopes of the Cl* atom, although slight differences might occur that result from a mass-dependent efficiency in the nonadiabatic transition of the perpendicular transition. Moreover, the fitting procedures were found to be insensitive to small variations (*ca.* 5%) in the values of the β parameters.

4. Results

Fig. 3 shows representative anisotropic TOF profiles for ^{35}Cl* and ^{37}Cl* atoms obtained from the photodissociation of Cl_2 at 320 nm and 340 nm, together with the fit obtained using the basis

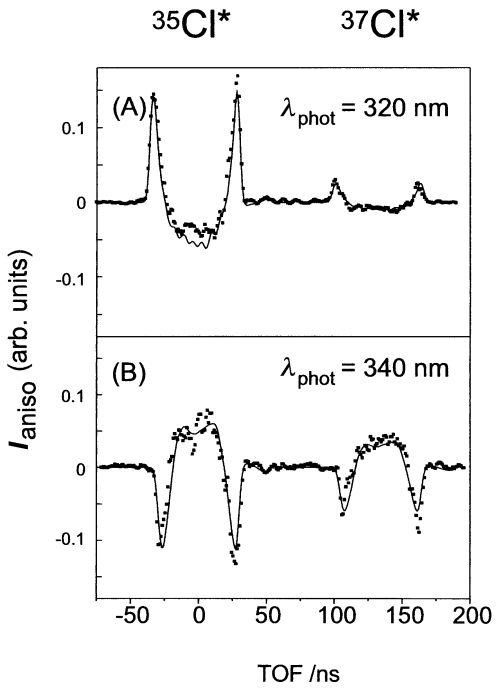

Fig. 3 Anisotropic composite time-of-flight profiles, $\boldsymbol{I}_{\text{aniso}}$ (solid squares) for ^{35}Cl* and ^{37}Cl* photofragments from the photodissociation of Cl_2 at (A) 320 nm and (B) 340 nm. Solid lines in (A) and (B) represent fits to the data using basis functions, $\boldsymbol{B}_{\text{aniso}}$ generated by Monte-Carlo simulation: see text for details.

functions generated by Monte-Carlo simulations. The anisotropic TOF profile, $\boldsymbol{I}_{\text{aniso}}$, at a photolysis wavelength of 320 nm shows the characteristic shape of a positive Im[$\boldsymbol{a}_1^{(1)}(\parallel,\perp)$] parameter, whereas at 340 nm, $\boldsymbol{I}_{\text{aniso}}$ reflects negative values for both ^{35}Cl* and ^{37}Cl* photofragments. Positive and negative signs of the orientation moment correspond to a preference for $\boldsymbol{J}$ pointing along $+y$ ("topspin") and $-y$ ("backspin") directions respectively. It is worthwhile to note that the ground-state Cl atom generated simultaneously with Cl* would be expected to have an orientation equal and opposite to its partner Cl* fragments so that angular momentum is conserved. However, for the present experiment, measurement of ground-state Cl atom orientation is rendered impracticable because of a limited instrumental resolution and the much larger Cl signal generated from photolysis on the C state alone. Indeed, the ratio of photodissociation cross-sections for C and B states, σ(C)/σ(B), is estimated to be about 170 at 350 nm excitation, and increases drastically at shorter wavelengths.[17]

Analysis of TOF profiles at a photolysis wavelength of 320 nm gives Im[$\boldsymbol{a}_1^{(1)}(\parallel,\perp)$] = 0.14 ± 0.1 for ^{35}Cl* and 0.07 ± 0.1 for ^{37}Cl*: the mass dependence of the orientation is caused by the difference in de Broglie wavelengths associated with the two isotopes. The results of repeated measurements of Im[$\boldsymbol{a}_1^{(1)}(\parallel,\perp)$] over the photolysis wavelength range of 270–400 nm are plotted in Fig. 4(B). The plot of Im[$\boldsymbol{a}_1^{(1)}(\parallel,\perp)$] as a function of photolysis wavelength has the form of a sinusoidal curve modulated by an envelope. The envelope has maximum amplitude at around 330 nm and decays at longer and shorter wavelengths. Photolysis below 270 nm and above 400 nm does not produce any observable orientation of the photofragments. Also, note the "phase lag" between the ^{35}Cl* and the ^{37}Cl* photofragments in the oscillation of Im[$\boldsymbol{a}_1^{(1)}(\parallel,\perp)$]. This behavior, again, is caused by the difference in de Broglie wavelengths associated with the two chlorine isotopes.

The Im[$\boldsymbol{a}_1^{(1)}(\parallel,\perp)$] parameter can be roughly modeled[23] as $\sin\{\alpha\sqrt{m}[\sqrt{E}-\sqrt{E-\Delta V}]\}$, where E is the total energy available to the photofragment of mass m, and ΔV is the average difference of potential energy for parallel and perpendicular transitions within a characteristic interaction range, α. The difference in the de Broglie wavelengths for the two isotopes at a given total energy

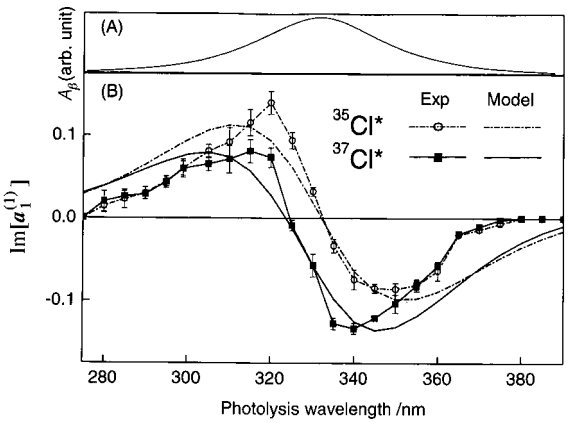

Fig. 4 (A) The envelope of oscillation as a function of the change in β parameter (β) over the photolysis wavelength range, modeled by $A_\beta = \sqrt{(1+\beta)(1-\beta/2)}$. (B) Experimentally determined Im[$\boldsymbol{a}_1^{(1)}(\|,\perp)$] parameters for ^{35}Cl* (open circle) and ^{37}Cl* (solid square) as a function of photolysis wavelength. Error bars represents one standard deviation derived from replicate measurements. Also shown are the results of the model calculation for ^{35}Cl* (dash–dot lines) and ^{37}Cl* (solid lines): see text for details.

causes a difference in the period of oscillation of the orientation parameter, which appears as a $\sqrt{m}$ dependence in the above expression.

Compared with the previous measurements of (ground-state) Cl-atom orientation in the photodissociation of ICl,[14,15] the period of oscillation of Im[$\boldsymbol{a}_1^{(1)}(\|,\perp)$] for the Cl_2 photolysis is slow: the Im[$\boldsymbol{a}_1^{(1)}(\|,\perp)$] parameter changes sign only once over a photolysis wavelength range 270–400 nm. The change of $[\sqrt{E} - \sqrt{E-\Delta V}]$ as a function of E slows down and approaches zero as the excitation energy is increased; hence, the period of the oscillation of the orientation moment increases as the available energy is increased. In the photodissociation of ICl, the photolysis wavelengths used were just above the dissociation threshold, leading to rapid oscillations, whereas in Cl_2 photodissociation, the available energy for the Cl* fragment is much greater (3000–5000 cm^{-1}), leading to a much slower oscillation of Im[$\boldsymbol{a}_1^{(1)}(\|,\perp)$]. The envelope of the oscillation reaches its maximum amplitude at around 330 nm and decays on either side. The behavior of the envelope agrees with our picture of interference between dissociative motion on the parallel and perpendicular surfaces: the amplitude is maximum when the two contributing components are equal in magnitude and it dies out as one of the components dominates the other. The envelope of the oscillation can be modeled as the geometric mean of contributions from parallel and perpendicular transitions: $A_\beta = \sqrt{(1+\beta)(1-\beta/2)}$. Fig. 4(A) show a plot of A_β as a function of wavelength in which the wavelength-dependent β parameter has been interpolated from the experimental measurements of Samartzis *et al.*[17] The calculated envelope correctly predicts the position of the maximum amplitude of oscillation.

To model the observed behavior of Cl* photofragment orientation, we assume that the perpendicular transition component of Cl* originates from initial excitation to the C state, followed by a nonadiabatic transition to the B state to give Cl + Cl*. At present, the matrix elements that would be required to accurately model the nonadiabatic radial derivative coupling are not available, although recent calculations[24] suggest that this type of nonadiabatic coupling may be of great importance. Furthermore, the recent experimental work of Samartzis *et al.*[17] indicates a curve crossing probability that decreases with increasing photofragment kinetic energy, which is at variance with a radial derivative coupling model. For these reasons, we have employed a simple curve crossing model of the chlorine photodissociation using the available (adiabatic) *ab initio* potential energy curves of Yabushita[18] to provide a yardstick with which we can compare the experimental data.

We have modeled the nonadiabatic transition with a single effective potential energy curve $V_{NA}(R)$, which switches smoothly from the C state to the B state, by employing a phenomenological coupling element that has the form of a Gaussian function with half-width at half-maximum of 0.42 Å centered on the curve crossing point $R_x = 3.16$ Å. The amplitude of this coupling term was

varied to produce an acceptable fit to the experimental data. The radial Schrödinger equation was solved numerically[25] on the $V_B(R)$ and on the $V_{NA}(R)$ potentials, and the phases of the radial wave functions, ϕ_B and ϕ_{NA}, were evaluated at the asymptote. In Fig. 4(B), the experimental $\mathrm{Im}[\boldsymbol{a}_1^{(1)}(\|,\perp)]$ is compared with $A_\beta \sin(\phi_B - \phi_{NA})$ obtained from the calculations. As can be seen in Fig. 4(B), the model calculation correctly predicts the phase shift between the two isotopes and the general energy dependence of the orientation moment, although it gives a somewhat broader envelope than experimentally observed. From an experimental viewpoint, the discrepancy between the experimental and theoretical envelopes might arise from the occurrence of another dissociating state with either parallel or perpendicular character, although the discrepancy may reflect systematic errors in the measurement of the translational anisotropy. Our model of envelope of oscillation is based on the interference between two dissociating states, and even a minute contribution of another state can affect the envelope of oscillation.

The effect of including a centrifugal potential in the calculations, which can be modeled by $N(N+1)\hbar^2/2\mu R^2$(where N is the nuclear rotational quantum number, μ is a reduced mass of diatomic molecule, and R is a internuclear distance), was found to be negligible. Overall, the simple crossing model calculations appear able to reproduce the qualitative, general features of the observed oscillation of the orientation moment, but fail to give a full quantitative agreement.

5. Discussion

For a mixed transition in which two dissociating states are accessed *via* parallel and perpendicular transitions respectively, the overall transition dipole moment vector, $\boldsymbol{\mu}$, lies between the parallel and perpendicular axes. Classically, the transition dipole moment vector can be viewed as an oscillating electric dipole, the initial direction of which is determined by the polarization of the photolysis light, $\boldsymbol{\varepsilon}_{phot}$. The transition dipole moment vector depends parametrically on the internuclear separation, R, and on the phase of the radial part of the dissociating wave function. As is shown schematically in Fig. 5(A), the initially prepared transition dipole moment can be decomposed into a parallel component, μ_z, and a perpendicular component, μ_x. Each component experi-

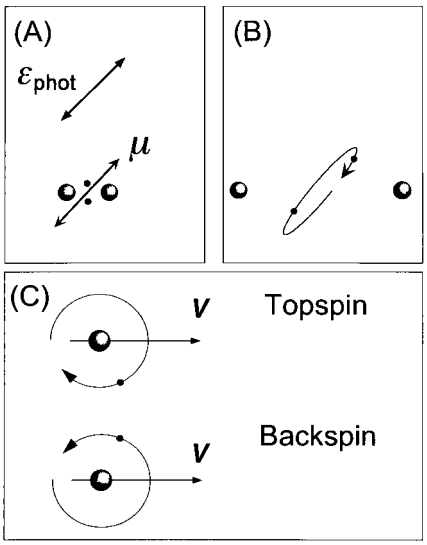

Fig. 5 Schematic view of a classical interpretation of orientation resulting from excitation to a mixed transition: (A) excitation with linearly polarized light induces oscillating electric dipole of electrons. (B) as the dissociation proceeds, parallel and perpendicular components of the transition dipole acquire a phase difference $\Delta\phi$, which induces a circular component in the oscillating transition moment. (C) at infinite separation of photofragments the net phase difference, $\Delta\phi$, can be non-zero, *i.e.*, the separated fragments each retain some circularity. Positive and negative signs of the orientation parameter correspond to "topspin" and "backspin" of the photofragments, respectively.

ences a different potential energy surface during the subsequent dissociation, and hence a phase difference ($\Delta\phi$) between the oscillations of the parallel and perpendicular components is acquired as the internuclear distance increases. The phase difference $\Delta\phi$ between the two oscillating electric dipoles leads to a circular component (helicity) in the motion of the electronic charge distribution, *i.e.*, a net electronic angular momentum above or below the plane containing $\boldsymbol{\varepsilon}_{\mathrm{phot}}$ and $\boldsymbol{v}$: see Fig. 5(B). At infinite separation of the photofragments, where the two potential energy surfaces converge to the same product asymptote, the phase difference $\Delta\phi$ also converges to its final value. The asymptotic phase difference, and the out-of-plane component of the angular momentum, are determined by the exact shapes of the potential energy curves encountered by each of the parallel and perpendicular components during motion along the dissociation pathway: see eqn. (2) and Fig. 5(C).

The above model gives an intuitive physical picture of the development of helicity as a phase difference between two orthogonal oscillations. This picture does not represent the actual experimental situation, however, because the dissociation process cannot simply be viewed as the motion of fragments with well-defined positions that develop as a function of time. Such a picture would be more applicable to wavepackets that can be excited using femtosecond laser pulses.[26] For a physical understanding of the present experiment, we must turn to a picture of a quasi steady-state excitation to the dissociation continuum, as that which would be obtained, for example, using a nanosecond excitation pulse. Indeed the present experiments rely on our ability to excite and probe a set of energetically well-defined continuum wavefunctions with an outgoing boundary condition, enabling us to measure their asymptotic radial phase difference.

The simple model calculations of the nonadiabatic transition presented in Section 4 do not fully reproduce the experimentally observed energy dependence of the Cl* atom photofragment orientation. The coupling matrix element for the nonadiabatic transition was arbitrarily chosen to be independent of the kinetic energy of the photofragment and localized at the crossing point. In general, nonadiabatic coupling matrix elements are kinetic energy dependent and the range of nonadiabatic interactions are nonlocal. Although our use of a phenomenological (gaussian shaped) nonadiabatic coupling based on a curve crossing mechanism can reproduce qualitatively the experimental data, this fact does not validate the curve crossing mechanism for Cl* generation in Cl_2 photodissociation. A more complete knowledge of the nonadiabatic (both curve crossing and radial derivative type) coupling matrix elements, along with the corresponding potential energy curves, is required to produce a more complete model of this system. We hope that revised theoretical calculations, along with the experimental measurements of the Cl* atom photofragment orientation and translational anisotropy, will allow a more detailed understanding of the mechanism behind nonadiabatic interaction in the photodissociation of molecular chlorine.

In conclusion, the outlook for applying measurements of (coherent) angular momentum orientation to photodissociation in other systems seems very bright. The technique is relatively simple and straightforward to carry out, the photofragment orientation is highly sensitive to mixing between states of different symmetries, and the interpretation of the results seems to offer insight into the photodissociation dynamics not readily discernible from the measurement of other parameters that do not contain quantum phase information.

We are most grateful to S. Yabushita for providing us with his *ab initio* potential energy curves, and to T. N. Kitsopoulos and D. H. Parker for providing us with a preprint of their work prior to publication. SAK thanks the US National Science Foundation for a predoctoral fellowship, and gratefully acknowledges receipt of a Dr. Franklin Veatch memorial fellowship. The funding for this work was provided by the US National Science Foundation under grant No. CHE-93-22690.

References

1 R. N. Zare and D. R. Herschbach, *Proc. IEEE*, 1963, **51**, 173.
2 R. N. Dixon, *J. Chem. Phys.*, 1986, **85**, 1866.
3 G. E. Hall and P. L. Houston, *Annu. Rev. Phys. Chem.*, 1989, **40**, 375.
4 R. J. van Brunt and R. N. Zare, *J. Chem. Phys.*, 1968, **48**, 4304.
5 O. S. Vasyutinskii, *Opt. Spectrosk.*, 1983, **54**, 524.
6 L. D. A. Siebbeles, M. Glass-Maujean, O. S. Vasyutinskii, J. A. Beswick and O. Roncero, *J. Chem. Phys.*, 1994, **100**, 3610.

7 K.-M. Chen and C.-C. Pei, *J. Chem. Phys.*, 1998, **109**, 6647.
8 O. S. Vasyutinskii, *Sov. Phys. JETP* (*Engl. Transl.*), 1980, **31**, 428.
9 E. W. Rothe, U. Krause and R. Duren, *Chem. Phys. Lett.*, 1980, **72**, 100.
10 J. Vigué, P. Grangier, G. Roger and A. Aspect, *J. Phys. Lett.*, 1981, **42**, L531.
11 A. T. J. B. Eppink, D. H. Parker, M. H. M. Janssen, B. Buijsse and W. J. van der Zande, *J. Chem. Phys.*, 1998, **108**, 1305.
12 T. P. Rakitzis and R. N. Zare, *J. Chem. Phys.*, 1999, **110**, 3341.
13 T. P. Rakitzis, S. A. Kandel and R. N. Zare, *J. Chem. Phys.*, 1998, **108**, 8291.
14 T. P. Rakitzis, S. A. Kandel, A. J. Alexander, Z. H. Kim and R. N. Zare, *Science*, 1998, **281**, 1346.
15 T. P. Rakitzis, S. A. Kandel, A. J. Alexander, Z. H. Kim and R. N. Zare, *J. Chem. Phys.*, 1999, **110**, 3351.
16 Y. Matsumi, K. Tonokura and M. Kawasaki, *J. Chem. Phys.*, 1992, **97**, 1065.
17 P. C. Samartzis, B. Bakker, T. P. Rakitzis, D. H. Parker and T. N. Kitsopoulos, *J. Chem. Phys.*, 1999, **110**, 5201.
18 S. Yabushita, 1998, unpublished results. The *ab initio* points are rescaled by a constant factor of 0.926 to match the bound part of B-state curve to the experimentally obtained B-state RKR potential energy curve, see J. A. Coxon, *J. Mol. Spec.*, 1980, **82**, 264.
19 A. J. Orr-Ewing and R. N. Zare, *Annu. Rev. Phys. Chem.*, 1994, **45**, 315.
20 R. N. Zare, *Angular Momentum, Understanding Spatial Aspects in Chemistry and Physics*, Wiley-Interscience, New York, 1988.
21 A. C. Kummel, G. O. Sitz and R. N. Zare, *J. Chem. Phys.*, 1986, **85**, 6874.
22 W. R. Simpson, A. J. Orr-Ewing, S. A. Kandel, T. P. Rakitzis and R. N. Zare, *J. Chem. Phys.*, 1995, **103**, 7299.
23 For this model we have assumed that the potential energy curves are of a square well type, with infinite wall at $R = 0$, see also ref. 14.
24 S. Yabushita, 1999, personal communication.
25 B. R. Johnson, *J. Chem. Phys.*, 1977, **67**, 4086.
26 It might be wondered what information would be yielded by a femtosecond pump–probe experiment. Such an experiment could, in principle, distinguish between and follow the two different dissociation pathways, because the wavepackets on the two different surfaces take a different time to separate into asymptotic fragments. In this case, however, the interference effect is removed because the different pathways can be distinguished. An intermediate regime occurs in which the interference would appear, but its description would depend sensitively on the temporal forms of the pump and probe pulses. For a cogent discussion of what is prepared in a bound-to-continuum transition, see J. L. Kinsey and B. R. Johnson, *J. Phys. Chem. A*, 1998, **102**, 9660.

Paper 9/01828J